Effects of Warpage on Fatigue Reliability of Solder Bumps: Experimental and Analytical Studies

Wei Tan, I. Charles Ume, Ying Hung, and C. F. Jeff Wu

***Abstract*—Out-of-plane displacement (warpage) has been a major thermomechanical reliability concern for board-level electronic packages. Printed wiring board (PWB) and component warpage results principally from coefficient of thermal expansion mismatch among the materials that make up the PWB assembly (PWBA). Warpage occurring during surface-mount assembly reflow processes and normal operations may lead to severe solder bump reliability problems. In this research, the effect of initial PWB warpage on the low cycle thermal fatigue reliability of the solder bumps in plastic ball grid array (PBGA) packages was studied using experimental and analytical methods. A real-time projection moiré warpage measurement system was used to measure the surface topology of PWBA samples at different temperatures. The thermal fatigue reliability of solder bumps was evaluated from experimental thermal cycling tests and finite element simulation results. Three-dimensional (3-D) models of PWBAs with varying board warpage were used to estimate the solder bump fatigue life for different types of PBGAs mounted on PWBs. In order to improve the accuracy of FE results, the projection moiré method was used to measure the initial warpage of PWBs, and this warpage was used as a geometric input to the finite element method. The simulation results were validated and correlated with the experimental results obtained using the projection moiré technique and accelerated thermal cycling tests. An advanced prediction model was generated to predict board level solder bump fatigue life based on the initial PWB warpage, package dimensions and locations, and solder bump materials.**

***Index Terms*—Fatigue, prediction model, solder bumps, warpage.**

I. Introduction

WARPAGE is one of the major thermomechanical reliability concerns for board-level electronic packaging. Printed wiring board (PWB) and component warpage results from coefficient of thermal expansion (CTE) mismatch among the materials that make up PWB assemblies (PWBAs) such as solder, copper, FR-4, encapsulation molding, and silicon. Warpage occurring during the surface-mount assembly reflow process and normal operations may cause serious reliability problems, such as severe solder bump fatigue failure, die cracking, and delamination of the solder bumps between electronic components and the PWB [1]. PWB/PWBA warpage can be measured by many different optical techniques, among which moiré methods have emerged as very accurate real-time, noncontact, full-field, superior techniques with high resolutions. In this paper, a warpage measurement system based on the projection moiré technique was used. The projection moiré method is complementary to the shadow moiré technique, and does not require a glass grating. Therefore, it is more suitable for measuring a PWB surface with assembled components, and it can easily be used to measure various board and package sizes by simply adjusting its grating sizes. The characteristics of the real-time projection moiré warpage measurement system are presented in this paper.

Fatigue is another common failure mechanism of electronic devices and is believed to be either fully or partially responsible for 90% of all structural and electrical failures. It is caused by cyclic thermomechanical stresses, and is severely affected by out-of-plane displacement of PWBs. This paper discusses the correlation between the initial PWB warpage and solder bump fatigue on board assemblies. The effect of the initial PWB warpage on the low cycle fatigue of the solder bumps on PBGA packages was studied in depth based on experimental study and finite element analysis. The projection moiré system and accelerated thermal cycling tests were used to evaluate the board level solder bump fatigue reliability affected by PWB warpage. Three-dimensional FE models of PWBAs with different initial board warpage were used to predict the solder bump fatigue life for different types of PBGAs on PWBs. Based on the experimental and simulation results, design of experiments and an advanced prediction model was developed to accurately investigate the correlation between the initial PWB warpage and solder bump fatigue life on board assemblies.

II. Projection Moiré Measurement System

A. Projection Moiré System Optical Setup

The projection moiré optical setup is shown in Fig. 1. A diode-pumped laser with a wavelength of 532-nm is expanded and then enters a Michelson interferometer to create the grating pattern on the sample surface. The interferometer's reference mirror is mounted on a piezoelectric transducer (PZT) for phase stepping to achieve high-resolution measurement. Two projected grating images captured by a charge-coupled device (CCD) camera at different time will be superposed to obtain moiré fringes. These fringes can then be used to calculate the surface topology of the PWB/PWBA. One image is the

Manuscript received March 07, 2008; revised June 07, 2009; accepted September 24, 2009. First published April 22, 2010; current version published May 05, 2010. This work was recommended for publication by Associate Editor C. Basaran upon evaluation of the reviewers comments.

W. Tan and I. C. Ume are with the School of Mechanical Engineering, Georgia Institute of Technology, Atlanta, GA 30332 USA (e-mail: gtg822r@mail.gatech.edu; charles.ume@me.gatech.edu).

Y. Hung and C. F. J. Wu are with the School of Industrial and System Engineering, Georgia Institute of Technology, Atlanta, GA 30332 USA (e-mail: yhung@isye.gatech.edu; jeffwu@isye.gatech.edu).

Color versions of one or more of the figures in this paper are available online at http://ieeexplore.ieee.org.

Digital Object Identifier 10.1109/TADVP.2010.2041451

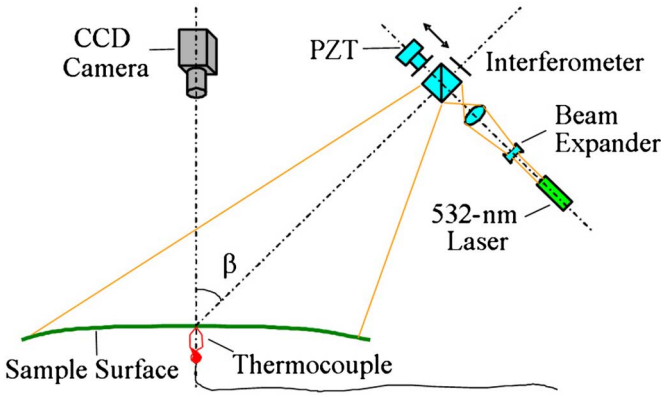

Fig. 1. Projection moiré optical setup.

reference grating pattern captured when the grating lines are projected onto a flat reference surface; the other image includes the deformed grating lines created by the PWB/PWBA surface being measured [2].

B. Out-of-Plane Displacement Calculation

The relationship between sample warpage and moiré fringes is shown below

$$w = \frac{np}{\tan\alpha + \tan\beta} \tag{1}$$

where w is out-of-plane displacement at the nth fringe order; n is fringe order; p is grating pitch; α observation angle; β is illumination angle.

For the projection moiré setup described above, the observation angle, α, is 0° and the illumination angle, β, is 45°. The fringe order, n, is not required to be an integer, and can be determined by $n = \text{phase}/2\pi$. To obtain accurate warpage results, four-step phase stepping method is applied to achieve precise fringe order [3]. Then warpage of the sample surface can be calculated.

The resolution of the projection moiré system depends on the surface size being measured. Normally the CCD camera with 480 × 512 pixels can resolve 100 fringes in its full field. The four-step phase stepping technique can increase the measurement resolution by 100 times. Therefore, if the size of a sample surface is $L \times L$, the resolution of the projection moiré measurement system is $L/10\,000$.

III. PWBA Test Vehicle

The PWBA test vehicle used in this research is shown in Fig. 2. It is composed of a 203.2 mm × 139.7 mm × 0.631 mm PWB and up to two PBGA packages per board. Two types of PBGA packages were used in this study: one has 256 solder bumps, a bump pitch of 1.27 mm, and dimensions of 27 × 27 mm; the other has 352 solder bumps, a bump pitch of 1.27 mm, and dimensions of 35 × 35 mm. As shown in Fig. 2, the PBGA can be located at a horizontal distance of 60 mm and a vertical distance of 30 mm from the center of the PWB, or at a horizontal distance of 0 mm and a vertical distance of 30 mm from the center of the PWB. The PWB consists of four copper layers

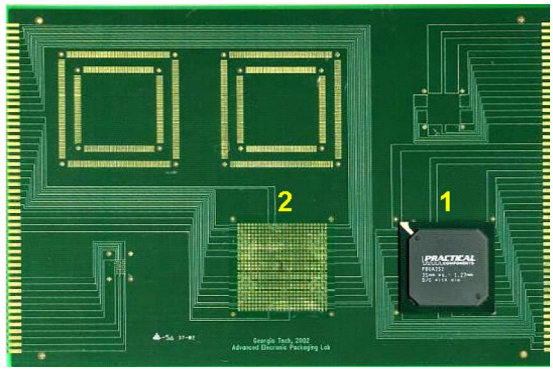

Fig. 2. PWBA test vehicle assembled with one 35 × 35 mm PBGA package.

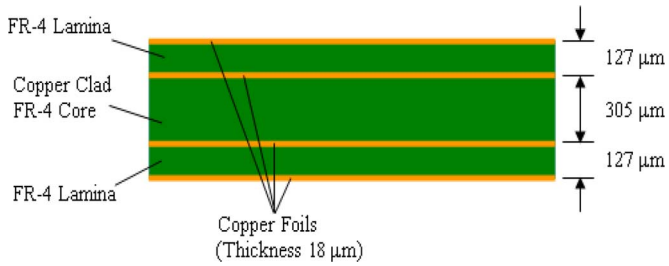

Fig. 3. Cross-section schematic of PWB test vehicle.

and three FR-4 layers. Fig. 3 shows a cross-section schematic of the layered PWB along with its thickness dimensions. Specifically, the top copper layer of the PWB contains traces, which are 127 μm thick and have a pitch of 508 μm.

IV. Experimental Study on Solder Bump Fatigue Reliability Affected by Initial PWB Warpage

In order to accurately set up a correlation between the initial PWB warpage and solder bump fatigue reliability on board assemblies, the accelerated thermal cycling tests were conducted using an ESPEC test chamber. The applied thermal cyclic condition was JESD22-A104-A with the temperature range between −40 °C and 125 °C every 20 min, keeping the dwell time as 10 min at the two temperature extremes.

There are a total of 20 PWBs assembled with 27 × 27 mm or 35 × 35 mm PBGA packages used in this study. The projection moiré system as shown in Fig. 1 was used to measure the warpage of the 20 PWBA samples at room temperature before the thermal cycling tests. Each PWB has different initial board warpage as shown in Table I. Five boards among the test vehicles were assembled with 27 × 27 mm PBGA packages at location 1 respectively, which was at a horizontal distance of 60 mm and a vertical distance of 30 mm from the PWB center; five PWBs were assembled with 27 × 27 mm PBGA packages at location 2, respectively, which was at a horizontal distance of 0 mm and a vertical distance of 30 mm from the PWB center; five PWBs were assembled with 35 × 35 mm PBGA packages at location 1, respectively; five PWBs were assembled with 35 × 35 mm PBGA packages at location 2, respectively. Fig. 4 shows the warpage measurement results for the PWBA with one 35 × 35 mm PBGA at Location 1 by using the projection moiré system.

TABLE I
INITIAL PWBA SAMPLE WARPAGE AT ROOM TEMPERATURE

Assembled Package Characteristics	27 × 27 mm PBGA, 63Sn-37Pb, 256 solder bumps		35 × 35 mm PBGA, 63Sn-37Pb, 352 solder bumps	
Package Location on PWB Sample	Location 1	Location 2	Location 1	Location 2
Max. Initial Warpage across PWB Sample 1 (Microns)	1706.4	1819.5	1754.2	1733.3
Max. Initial Warpage across PWB Sample 2 (Microns)	1997.0	2004.4	2022.7	2147.9
Max. Initial Warpage across PWB Sample 3 (Microns)	2109.8	2105.3	2098.1	2367.5
Max. Initial Warpage across PWB Sample 4 (Microns)	2433.3	3076.6	2536.6	2741.8
Max. Initial Warpage across PWB Sample 5 (Microns)	3176.1	3824.0	2878.3	3009.7

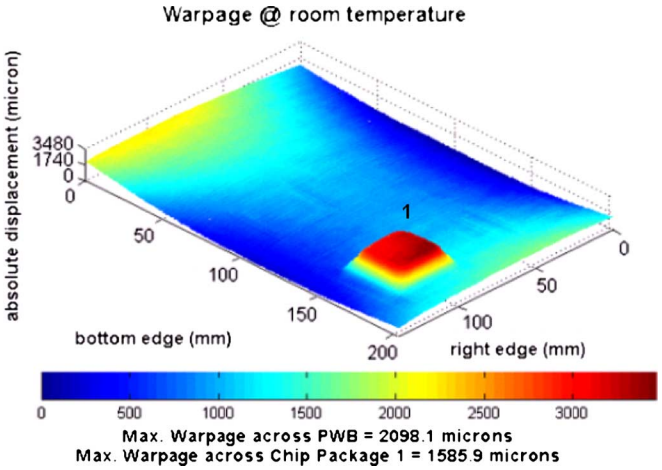

Fig. 4. Warpage measurement plot of PWBA with one 35 × 35 mm PBGA at location 1 using orojection moiré system.

All of the applied PBGA packages have daisy chain connections. The initial resistance for each PBGA package is shown in Table II.

The above PWBA samples were placed in the ESPEC test chamber to perform the standard thermal cycling test [JESD22-A104-A] with the temperature range from −40 °C to 125 °C. Total of 3000 thermal cycles were conducted. Each cycle has the time period of 60 min. Failure of the solder bumps is defined when the resistance value is larger than 300 Ω in this study. 300 Ω is used as a critical value to determine failure of solder bumps in a package because that is the value that was used by most researchers to determine the onset of solder bump failure.

The results of fatigue failures obtained from experiment are shown in Fig. 5. These experimental results show that the initial PWB warpage has significant effects on the low cycle fatigue life of solder bumps on PBGA packages. The higher the initial warpage, the lower the fatigue life of solder bumps on board assemblies. If the maximum initial warpage of the PWB sample changes from 1.706 mm to 3.176 mm, the Sn–Pb solder bump fatigue life of the 27 × 27 mm PBGA package assembled at location 1 is decreased by 28.4%, from 2900 cycles to 2075 cycles. If the maximum initial warpage of the PWB sample changes from 1.733 mm to 3.009 mm, the Sn–Pb solder bump fatigue life of the 35 × 35 mm PBGA package assembled at location 2 is decreased by 26.7%, from 2625 cycles to 1925 cycles. The dimensions and locations of packages also affect the bump fatigue. The solder bumps have longer fatigue life if the package is small in size and is located far from the PWB center. The PWB samples have large deformations near the board center. Therefore, if the electronic package is assembled far from the PWB center, the initial board warpage has less effect on the fatigue life of solder bumps on board assemblies.

During the thermal cycling test, the warpage of the 20 PWBA samples was measured using the projection moiré system after each set number of thermal cycles. Fig. 6 shows the relative warpage change across the PWBs during the thermal cycling test. Each curve represents the average values of the warpage change across five PWB samples populated with 27 × 27 mm PBGA or 35 × 35 mm PBGA, at locations 1 or locations 2. A comparison of the relative warpage changes is provided in the figure for four sets of samples. The experimental results show that as the number of thermal cycles increases, the PWB warpage increases. The assembled PBGA packages constrain the deformation of the PWB samples during thermal cycling process. For the 35 × 35 mm PBGA assembled at location 2, the maximum warpage across the PWB changed 25.7% after 3000 thermal cycles; while for the 35 × 35 mm PBGA assembled at location 1, the maximum warpage across the PWB changed 29.8% after 3000 thermal cycles; for the 27 × 27 mm PBGA assembled at location 2, the maximum warpage across the PWB changed 28.5% after 3000 thermal cycles; while for the 27 × 27 mm PBGA assembled at location 1, the maximum warpage across the PWB changed 33.4% after 3000 thermal cycles. A large size electronic package located near the board center will cause the PWB to warp less than if it were located further away from the center.

V. FINITE ELEMENT MODELING TO ESTIMATE FATIGUE LIFE OF SOLDER BUMPS AFFECTED BY INITIAL PWB WARPAGE

A. Geometric Modeling and Meshing

In order to study the effect of initial PWB warpage on the low cycle fatigue of solder bumps in PBGA packages, 3-D finite element models of PWBAs with different degrees of board warpage were used to estimate the solder bump fatigue life for different types of assembled PBGAs using ANSYS7.1. To improve the

TABLE II
INITIAL RESISTANCE OF DAISY CHAIN PBGA PACKAGES

Assembled Package Characteristics	27 × 27 mm PBGA, 63Sn-37Pb, 256 solder bumps		35 × 35 mm PBGA, 63Sn-37Pb, 352 solder bumps	
Package Location on PWB Sample	Location 1	Location 2	Location 1	Location 2
Resistance (Ω) of Package on PWB 1	0.3	0.3	0.2	0.2
Resistance (Ω) of Package on PWB 2	0.4	0.3	0.2	0.3
Resistance (Ω) of Package on PWB 3	0.3	0.2	0.2	0.2
Resistance (Ω) of Package on PWB 4	0.3	0.3	0.3	0.2
Resistance (Ω) of Package on PWB 5	0.2	0.3	0.2	0.2

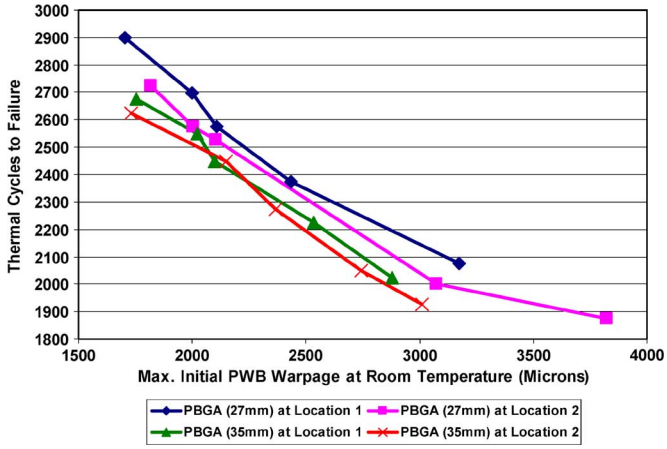

Fig. 5. Solder bump fatigue failure affected by initial PWB warpage.

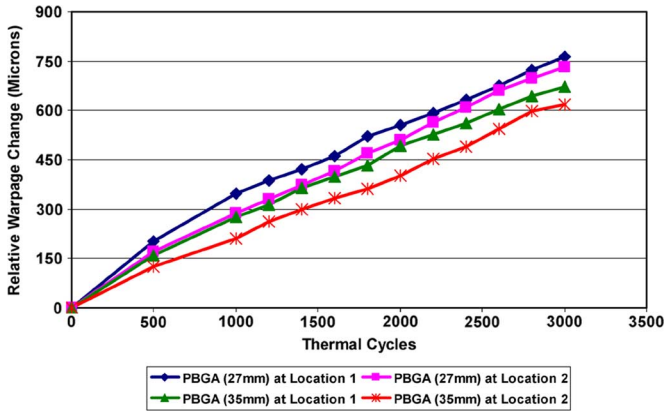

Fig. 6. Relative warpage change across PWBs during thermal cycling test.

accuracy of FEA solutions, the PWB warpage was measured using the projection moiré method at the temperatures of 183 °C and 217 °C. These two temperatures are the solder stress free and starting temperatures for the PWBA models with 63Sn-37Pb solder bumps and 95.5Sn-3.8Ag-0.7Cu solder bumps, respectively. Three PWB samples with different initial warpage values were used in this study. Table III shows the maximum warpage measurement values for the three PWB samples at different temperatures.

Based on the high resolution of the real-time projection moiré warpage measurement system, the warpage value at any location on the sample surface can be collected at each temperature level. In order to create a 3-D surface map of the PWB warpage, warpage was measured at 45 different locations on the PWB at the eutectic temperatures of 183 °C (Sn–Pb) and 217 °C (lead-free), respectively. Those measured points are distributed over the PWB surface uniformly. The warpage values for the 45 specified points were inputted into finite element method (FEM) to generate the accurate geometry of the PWB surface with warpage for each sample at each temperature level. SHELL91 elements were used to mesh the PWB surface for their advantages in modeling layered shell structures. Two types of PBGA packages, including package molding, BT substrate, and solder bumps, were modeled and meshed using SOLID95 elements, which are 3-D 20-node solid elements. Fig. 7 shows the meshed PWB with a 35 × 35 mm PBGA package.

B. Material Properties for Modeling

The material properties used in the PWBA models are shown in Tables IV and V [4]–[6]. Two types of solder bumps were simulated in the models: one is eutectic 63Sn-37Pb alloy, and the other is 95.5Sn-3.8Ag-0.7Cu alloy. They were both modeled as nonlinear, elastic-plastic-creep, isotropic, and temperature dependent. In order to obtain accurate simulation, temperature dependent material properties for Sn–Pb and lead-free solder obtained from the stress-strain curves in [5], [6] were used in the FE models.

C. Boundary Constraints and Thermal Cycling Tests

In the FEA model, the PWB length is in the X-direction, the PWB width is in the Y-direction, and the PWB thickness is in the Z-direction. Along the width directions (Y-directions) of the PWB, the Z-displacement in each node is zero, because during the testing, the PWB is supported on the width directions with two invar rods. Therefore, to prevent any motion of the PWBA, there is a constraint in the Z-direction along the width edges of the PWB. The FE simulation was utilized to investigate the solder bump fatigue reliability under the standard thermal cycle conditions [JESD22-A104-A], which is also used in the experimental study. The structure was assumed to be stress free at 183 °C for 63Sn-37Pb solder bumps, and at 217 °C

TABLE III
MAXIMUM WARPAGE VALUES ACROSS PWBS AT DIFFERENT TEMPERATURES

Temperature (°C)	Maximum Warpage of PWB Sample 1 (Microns)	Maximum Warpage of PWB Sample 2 (Microns)	Maximum Warpage of PWB Sample 3 (Microns)
25	2105.3	3076.6	3824.0
183	995.1	2158.9	3012.5
217	852.4	2008.2	2891.2

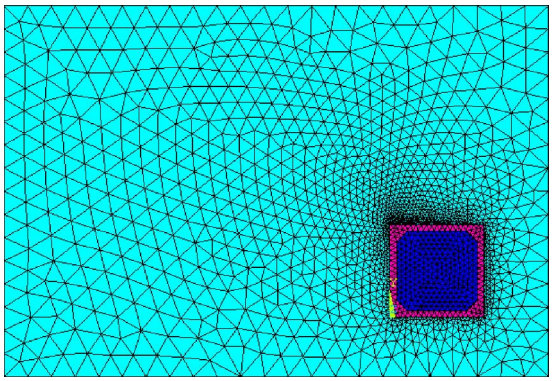

Fig. 7. Meshed PWB with 35 × 35 mm PBGA package.

for 95.5Sn-3.8Ag-0.7Cu bumps. It was cooled down from stress free temperatures (183 °C and 217 °C) to room temperature (25 °C) in 150 s. Ten complete thermal cycles were simulated.

D. Fatigue Prediction and Analysis

Based on the finite element models developed in previous sections, the fatigue life of Sn–Pb and lead-free solder bumps were predicted using effective strain solutions of the models after ten thermal cycles. The effective plastic strain of the solder bumps can be calculated according to (2) [7]

$$\varepsilon_{eff} = \frac{\sqrt{2}}{3}\sqrt{(\varepsilon_1-\varepsilon_2)^2+(\varepsilon_2-\varepsilon_3)^2+(\varepsilon_3-\varepsilon_1)^2} \quad (2)$$

where $\varepsilon_i (i = 1,2,3)$ are the principal strains.

The effective strain range is the difference in the two strains resulting from two extreme temperatures in each thermal cycle. The maximum effective strain value of the solder bumps was used for fatigue estimation. An empirical relationship between plastic strain and bump life, proposed by Coffin–Manson [8], has been widely used to predict solder bump fatigue life

$$\Delta\varepsilon_p = \varepsilon_f(2N_f)^c \quad (3)$$

where $\Delta\varepsilon_p$ represents the plastic strain range, N_f is the total number of cycles to failure, $\varepsilon_f (= 0.325)$ is the fatigue ductility coefficient, and $c (= -0.7 \sim -0.5)$ is the fatigue ductility exponent.

E. Model Validation

To validate the FE model, the PWB test sample with one 35 × 35 mm 63Sn-37Pb PBGA package shown in Fig. 2 was used. The FE model went through the first four temperature load steps in the thermal cycling simulation: from 183 °C to room temperature in 150 s, then heated up to 125 °C, while keeping the dwell time as 10 min at 25 °C and 125 °C. The PWB warpage entered into the FE model had a maximum value of 995.1 μm at 183 °C, which was the measurement result from the projection moiré experimental system using the corresponding PWB sample. At each end of the temperature load steps, the maximum PWB out-of-plane displacements from projection moiré experiments and FE model were compared and are shown in Table VI. This data shows that the maximum difference between experimental and modeling results is 7.8%. The FE model results agreed well with the corresponding experimental results, and can be used to study the correlation between PWB warpage and low cycle fatigue life of solder bumps on board assemblies.

F. Effect of PWB Warpage on Solder Bump Fatigue

In this section, the FE models developed in previous sections were used to study the fatigue life of solder bumps on board assemblies affected by initial PWB warpage. Two types of PBGA packages, 27 × 27 mm and 35 × 35 mm packages, were used. Each PBGA package has Sn–Pb and Sn-Ag-Cu solder bumps, and can be placed at three different locations: location 1 is at the PWB center, location 2 is at a horizontal distance of 60 mm and a vertical distance of 30 mm from the PWB center, and location 3 is at a horizontal distance of 78 mm and a vertical distance of 46 mm from the PWB center. The third location has the longest distance of 91 mm between the PWB center and package center. Based on the projection moiré measurement results, three different PWB samples as shown in Table III were modeled. The measured warpage values were entered into the FEM to improve the accuracy of the PWB surface geometry at the starting temperature. The shape of the PWB warpage, convex up $(+)$ or concave up $(-)$, was also considered as shown in Fig. 8, i.e., the PBGA package can be assembled on both sides of each PWB.

The fatigue assessment of the solder bumps with maximum strain on board assemblies for 27 × 27 mm and 35 × 35 mm PBGA packages with Sn–Pb and Sn-Ag-Cu solder are shown in Figs. 9–12. The FE simulation results are consistent with the above thermal cycling experimental results. For a PWB with higher initial warpage, the fatigue life of solder bumps on board assemblies is reduced. A PWB with concave shape will decrease the reliability of solder bumps more than a PWB with convex shape. In addition, lead-free solder bumps are much more reliable than Sn–Pb solder bumps [9].

TABLE IV
ROOM TEMPERATURE MATERIAL PROPERTIES USED FOR FE SIMULATION

Material		CTE (ppm/°C)	Elastic Modulus (GPa)	Property
PWB	FR-4	20.0	22.4	Linear Elastic, Orthotropic
	Copper Foil	18.9	79.5	Linear Elastic, Isotropic
Solder Bump	63Sn-37Pb	21.0	19.7	Non-Linear, Elastic-Plastic-Creep, Isotropic
	95.5Sn-3.8Ag-0.7Cu	21.0	50.3	
BT Substrate		15.0	14.0	Linear Elastic, Isotropic
Package Molding		17.5	15.0	Linear Elastic, Isotropic

TABLE V
TEMPERATURE DEPENDENT MATERIAL PROPERTIES USED FOR FE SIMULATION

Material	Temperature (°C)	CTE (ppm/°C)	Elastic Modulus (GPa)
FR-4	25	20	22.4
	95	20	20.7
	150	20	17.9
63Sn-37Pb	25	21	19.7
	125	21	11.7
95.5Sn-3.8Ag-0.7Cu	25	21	50.3
	125	21	25.3

TABLE VI
MAXIMUM PWB WARPAGE RESULTS OF EXPERIMENTS AND FE MODEL AT DIFFERENT TEMPERATURES

Temperature Load Steps	Max. PWB Warpage from Experiments (Microns)	Max. PWB Warpage from FE Model (Microns)	Differences
Initial 183 °C	995.1	980	1.5%
Cooling to 25 °C	2055.2	2196	-6.4%
Keeping 25 °C for 10min	2041.6	2193	-6.9%
Heating to 125 °C	1080.5	1172	-7.8%
Keeping 125 °C for 10min	1086.8	1171	-7.2%

Fig. 8. PWB warpage shape.

VI. DEVELOPMENT OF STATISTICAL ANALYSIS AND PREDICTION MODEL

A. Design of Simulations and Regression Model

In order to study the correlation between initial PWB warpage and solder bump fatigue reliability, a five-factor design of simulations and a regression model were developed for Sn–Pb and lead-free solder bumps based on the FEA solutions. In the regression model, the response is the fatigue life time of solder bumps; the factors of interest are the maximum initial PWB warpage at room temperature, warpage shape, PBGA package dimension, location of package, and solder bump material. The PWB warpage shape can be convex up (+1) or concave up (−1).

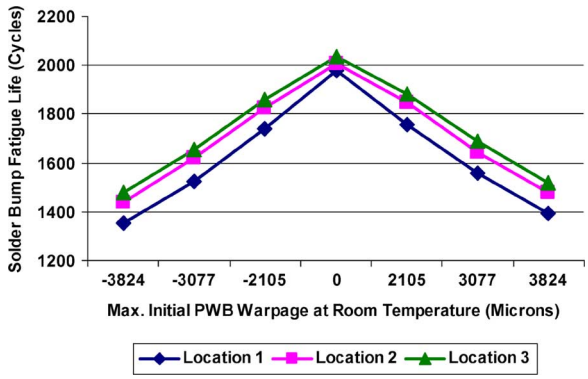

Fig. 9. Sn–Pb solder bump fatigue assessment of 27 × 27 mm PBGA on different PWB locations.

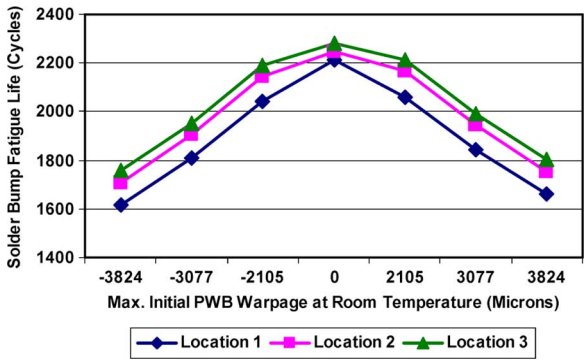

Fig. 10. Lead-free solder bump fatigue assessment of 27 × 27 mm PBGA on different PWB locations.

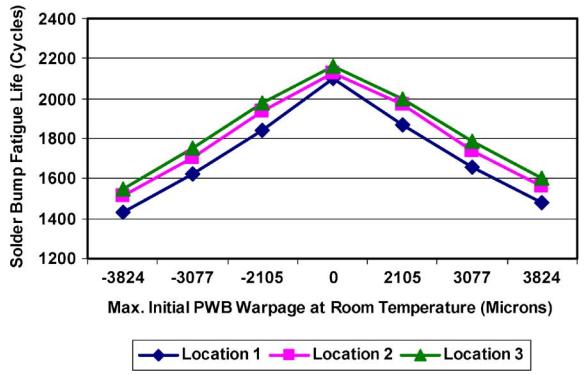

Fig. 11. Sn–Pb solder bump fatigue assessment of 35 × 35 mm PBGA on different PWB locations.

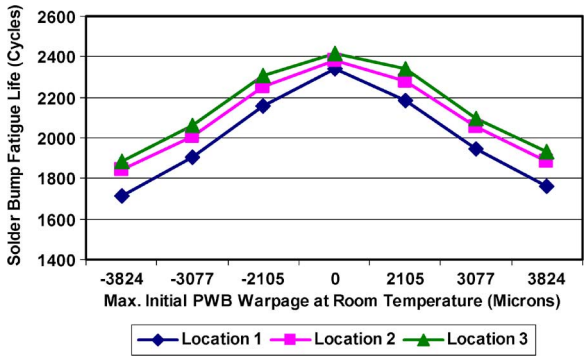

Fig. 12. Lead-free solder bump fatigue assessment of 35 × 35 mm PBGA on different PWB locations.

The length of the package, which represents its longest side, is always referred to as the dimension of the package, d_p. The location of the package is determined from the PWB center to the package center. In (4), whenever the solder bump material is Sn–Pb, "-1" is substituted for m_s, and whenever the bump material is Sn-Ag-Cu, "$+1$" is substituted for m_s. Equation (4) shows a reduced bilinear model expressing the response as a function of the five predictor variables and their two-factorial interactions [10]

$$N_r = 1855 - 165w_{\max} + 12d_p + 148m_s + 5.94w_{\max}w_{\text{shape}} + 0.219w_{\max}l_p + 0.0263d_pl_p \quad (4)$$

where N_r is fatigue life estimation of solder bumps (cycles); $w_{\max}$ is maximum initial PWB warpage at 25 °C(mm); w_{shape} is warpage shape; d_p is package dimension (mm); l_p is location of package (mm); m_s is solder bump material.

B. Advanced Model Fitting Based on FE Simulation Results

Regression analysis in Section IV-A is intuitive and simple. However, there are some drawbacks. First, linear regression models usually assume random errors in the output. This is not true for most of the FE simulations because they usually yield a deterministic answer for a given set of inputs. Second, the underlying system may be very complicated which can not be well approximated by the simple linear model. Therefore, more flexible nonlinear metamodels (prediction models) are called for.

The kriging model is the most popular method used for obtaining metamodels based on computer simulations [11]. It is popular because it obtains interpolating metamodels which are suitable for conducting deterministic simulations. Assume the true function $N_k(\vec{x})(\vec{x} \in R^p)$, is a realization from a stochastic process. A commonly used kriging model, known as ordinary kriging, can be stated as follows:

$$N_k(\vec{x}) = \mu_0 + Z(\vec{x}) \quad (5)$$

where μ_0 is an unknown parameter, and $Z(\vec{x})$ is a weak stationary stochastic process with a mean of 0 and a covariance function of $\sigma^2\psi$.

To calculate the metamodel (or predictor), assume that the true function is evaluated at m inputs $\{\vec{x}_1, \ldots, \vec{x}_m\}$, and $N_{\text{out}} = (N_1, \ldots, N_m)^T$ is the corresponding outputs. For an unobserved input x, the ordinary kriging predictor is shown in

$$\hat{N}_k(\vec{x}) = \hat{\mu}_0 + \varphi(\vec{x})^T\Psi^{-1}(N_{\text{out}} - \hat{\mu}_0 I) \quad (6)$$

where I is a column of 1's with a length of m, $\varphi(\vec{x}) = (\psi(\vec{x} - \vec{x}_1), \ldots, \psi(\vec{x} - \vec{x}_m))^T$, Ψ is an $m \times m$ matrix with the ijth element of $\psi(\vec{x}_1 - \vec{x}_j)$, and $\hat{\mu}_0 = I^T\Psi^{-1}N_{\text{out}}/I^T\Psi^{-1}I$.

The most popular correlation function, Gaussian product correlation function is used in this research to solve for φ in kriging model as shown in

$$\psi(\vec{h}) = \exp\left(-\sum_{j=1}^{p}\theta_j h_j^2\right), \quad \Theta = (\theta_1, \cdots, \theta_p)^T. \quad (7)$$

In order to better understand the effect of the package assembly location in this research, three different locations were investigated with their exact coordinates in horizontal direction and vertical direction (Hl_p and Vl_p) with respect to the PWB center. In addition, one more factor was added into the prediction model to denote the existence of initial PWB warpage. Therefore, a total of seven factors $(p = 7)$ were considered in the kriging model. These factors are denoted by the vector $\vec{x}$. The correlation parameters (coefficients of the factors in $\vec{x}$ vector), Θ, were estimated by maximizing the likelihood as shown in (8) [11]. These correlation parameters (coefficients) used in the

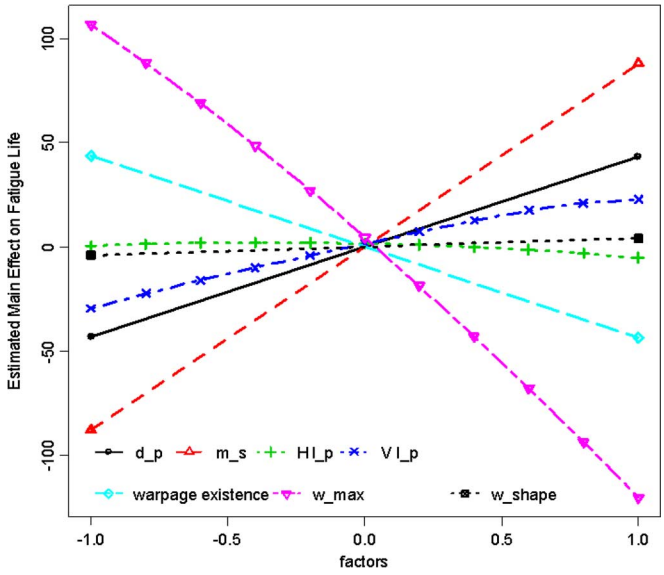

Fig. 13. Main effect plot of seven factors on solder bump fatigue reliability.

kriging predictor in (9) which are shown below were obtained from finite element simulation results

$$\begin{aligned}
&\theta_1(\text{package dimension}) = 0.01\\
&\theta_2(\text{solder bump material}) = 0.01\\
&\theta_3(\text{horizontal location of package}) = 0.01\\
&\theta_4(\text{vertical location of package}) = 0.17\\
&\theta_5(\text{warpage existence}) = 4.28\\
&\theta_6(\text{maximum initial PWB warpage}) = 0.01\\
&\theta_7(\text{warpage shape}) = 0.04\\
&\hat{\Theta} = (0.01, 0.01, 0.01, 0.17, 4.28, 0.01, 0.04)^T \qquad (8)\\
&\hat{\mu}_0 = 1101.6 \text{ was obtained from finite}\\
&\quad \text{element simulation results.}\\
&\hat{N}_k(\vec{x}) = 1101.6 + \varphi(\vec{x})^T \Psi^{-1}(N_{\text{out}} - 1101.6I) \qquad (9)
\end{aligned}$$

In order to study the effects of different factors on the thermal fatigue reliability of solder bumps, the sensitivity analysis technique was applied on the ordinary kriging predictor as shown in (9). Fig. 13 shows the effects of the seven different factors. In Fig. 13, the value of -1 for the warpage existence means there is no initial warpage on the PWB; while the value of 1 means that the initial warpage exists on the PWB. With the occurrence of initial board warpage, the solder bump fatigue reliability is significantly decreased. By increasing the maximum warpage across the PWB $(w_{\max})$ from the value of -1 to 1, the solder fatigue life is constantly decreased. For the solder materials (m_s), Fig. 13 shows that the lead-free solder with the value of 1 is more reliable than the Sn–Pb solder with the value of -1. Also, the package dimension (d_p) has some effects on the solder bump fatigue life. The package location (Hl_p, Vl_p) and PWB warpage shape have small effects on the solder bump reliability. Moreover, there are two significant interactions between the PWB warpage and solder materials as shown in Fig. 14. The

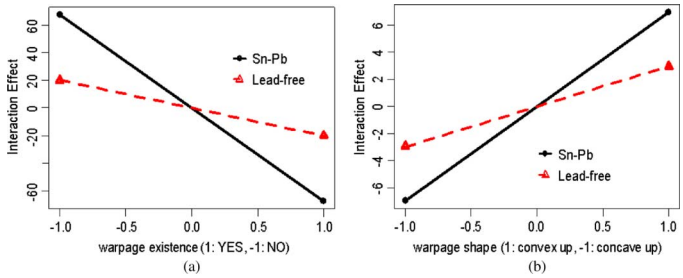

Fig. 14. Two significant interactions between PWB warpage and solder materials.

effect of PWB warpage on the fatigue life is higher with Sn–Pb solder than with lead-free material. Compared with the lead-free solder, Sn–Pb solder can produce more effects on the fatigue life when the warpage shape is changed.

C. Analysis of Advanced Integrating Model

In the previous sections, the effect of initial PWB warpage on solder bump fatigue reliability was studied based on FE simulation results. However, the simulation results are not as accurate as the experimental results. In order to effectively integrate the simulation and experimental data, a location adjustment model was developed as shown in (10) [12]. The idea is to first fit a Gaussian process model using only the simulation results, and then adjust this model by limited physical experimental results

$$N_f(\vec{x}) = N_k(\vec{x}) + \delta(\vec{x}) + err \qquad (10)$$

where $N_f(\vec{x})$ represents the experimental results, $N_k(\vec{x})$ represents the FE simulation results, err is an additive error which follows a normal distribution with a mean of 0 and a variance of σ^2, and $\delta(\vec{x})$ is the location adjustment term.

In practice, the $N_f(\vec{x})$ and $N_k(\vec{x})$ may not share the same input values. This problem can be easily overcome by replacing $N_k(\vec{x})$ with $\hat{N}_k(\vec{x})$ estimated by (9). The location adjustment term is estimated by $\delta(x) = 1830.3 - 540 w_{\max}$ using the forward selection technique with R^2 at 0.7. Therefore, the final integrated model to predict solder bump fatigue life was obtained as shown in

$$\hat{N}_f(\vec{x}) = 2931.9 - 540 w_{\max} + \varphi(\vec{x})^T \Psi^{-1}(N_{\text{out}} - 1101.6I). \qquad (11)$$

This advanced integrating model is effectively optimized with the experimental data of Sn–Pb solder bump fatigue life discussed in Section IV. It has higher accuracy to evaluate the bump reliability than the prediction model in (4) and (9). Based on the kriging model shown in (11), solder bump fatigue reliability was predicted and compared with the experimental results from the accelerated thermal cycling tests. Table VII shows four different comparisons. The maximum difference in solder bump fatigue life between the kriging prediction model and the experimental results is 6.1%. Therefore, the kriging prediction model as shown in (11) is able to successfully estimate the solder bump fatigue reliability affected by PWB warpage with very high accuracy. To further increasing the accuracy of the advanced prediction model in (11), more experimental fatigue reliability data of lead-free solder bumps and data comparisons are needed.

TABLE VII
SOLDER BUMP FATIGUE RELIABILITY COMPARISON BETWEEN PREDICTION MODEL AND EXPERIMENTS FOR DIFFERENT CASES

Case	1	2	3	4
Max. Initial Warpage across PWB at Room Temperature (mm)	1.833	2.013	2.171	2.425
PBGA Dimension (mm)	27×27	27×27	35×35	35×35
Distance from PBGA Center to Board Center (mm)	67	30	67	30
Fatigue Life from Prediction Model (Cycles)	2633	2465	2507	2277
Experimental Fatigue Life (Cycles)	2750	2625	2400	2250
Difference	-4.3 %	-6.1 %	4.4 %	1.2 %

VII. CONCLUSION

In this research, the effect of initial PWB warpage on the low cycle fatigue of the solder bumps on PBGA packages was studied based on the projection moiré measurement system and finite element modeling. This study successfully documents the correlation between initial PWB warpage and fatigue reliability of solder bumps on board assemblies. The projection moiré system and accelerated thermal cycling tests were used to investigate how initial PWB warpage affects the solder bump fatigue on board assemblies. The experimental results show that for a PWB with higher initial warpage, the fatigue life of solder bumps on board assemblies is reduced. The solder bumps have longer fatigue life if the package is small in size and is located far from the PWB center. In addition, with increasing the number of thermal cycles, the PWB warpage increases. The assembled PBGA packages constrain the deformation of the PWB samples during thermal cyclic conditions. Meanwhile, 3-D FE models were developed to predict the solder bump fatigue reliability affected by initial PWB warpage. The simulation results are consistent with the above experimental results. They also show that a PWB with concave shape will decrease the reliability of solder bumps more than a PWB with convex shape. The dimensions and locations of packages, and solder bump materials also affect the bump fatigue life. The above guidelines can be used to estimate the thermomechanical reliability of solder bumps on board assemblies with initial PWB warpage.

Design of experiments and an advanced prediction model were developed to study the correlation between initial PWB warpage and solder bump fatigue reliability based on experimental results and the FEA solutions. An advanced kriging model was developed and used to investigate the effects of initial PWB warpage on solder bump thermal fatigue reliability with very high accuracy.

REFERENCES

[1] C. P. Yeh, K. Banerjee, and T. Martin *et al.*, "Experimental and analytical investigation of thermally induced warpage for printed wiring boards," in *Proc. 41st Electron. Compon. Technol. Conf.*, 1991, pp. 382–387.
[2] H. Ding, R. E. Powell, and I. C. Ume, "A projection moiré system for measuring warpage with case studies," *Int. J. Microcircuits Electron. Packag.*, vol. 25, no. 1, pp. 15–26, 2003.
[3] H. Ding, R. E. Powell, C. H. Hanna, and I. C. Ume, "Warpage measurement comparison using shadow moiré and projection moiré methods," *IEEE Trans. Compon. Packag. Technol.*, vol. 25, no. 4, pp. 714–721, 2002.
[4] Y. Polsky and I. C. Ume, "Thermoelastic modeling of a PWB with simulated circuit traces subjected to infrared reflow soldering with experimental validation," *J. Electron. Packag.*, vol. 121, pp. 1–8, 1999.
[5] H. L. J. Pang, B. S. Xiong, and F. X. Che, "Modeling stress strain curves for lead-free 95.5Sn-3.8Ag-0.7Cu solder," in *Proc. 5th Int. Conf. Thermal Mechan. Simulat. Experiments Micro-Electronics Micro-Systems*, 2004, pp. 449–453.
[6] F. X. Che and H. L. J. Pang, "Thermal fatigue reliability analysis for PBGA with Sn-3.8Ag-0.7Cu solder joints," in *Proc. 2004 Electron. Packag. Technol. Conf.*, 2004, pp. 787–792.
[7] Q. Yao, J. Qu, and S. X. Wu, "Estimate the thermomechanical fatigue life of two chip scale packages," in *Proc. 49th Electron. Compon. Technol. Conf.*, 1999, pp. 797–802.
[8] V. Gektin, A. Bar-Cohen, and J. Ames, "Coffin-manson fatigue model of underfilled flip chips," *IEEE Trans. Compon., Packag., Manuf. Technol.*, vol. 3, pp. 317–326, Sep. 1997.
[9] W. Tan and I. C. Ume, "Fatigue assessment of solder bumps on board assemblies affected by PWB warpage," *IMAPS J. Microelectron. Electron. Packag.*, vol. 4, no. 1, pp. 37–44, 2007.
[10] C. F. J. Wu and M. Hamada, *Experiments: Planning, Analysis, and Parameter Design Optimization*. New York: Wiley, 2000.
[11] T. J. Santner, B. J. Williams, and W. I. Notz, *The Design and Analysis of Computer Experiments*. New York: Springer, 2003.
[12] Z. Qian, C. C. Seepersad, V. R. Joseph, J. K. Allen, and C. F. J. Wu, "Building surrogate models based on detailed and approximate simulations," *ASME J. Mechan. Design*, vol. 128, pp. 668–677, 2006.

Authors' photographs and biographies not available at the time of publication.